Journal of the Korean Nuclear Society
Volume 12, *Number* 4, *December*, 1980

《**Original**》

Dynamic Characteristics of Fuel Rods

Hae Lee

Korea Atomic Energy Research Institute
(Received October 16, 1980)

Abstract

The dynamics of a typical PWR fuel rod are investigated. Mathematical models of the support grid and fuel rod were derived and verified experimentally. The finite element model and SAP V computer program were used to calculate the natural frequencies and mode shapes. A singlespan beam model is also given for predicting the fundamental mode dynamics of prototype fuel rods. The results agree quite well with the finite-element model results.

요 약

核燃料棒의 動特性을 究明하였다. 支持그릴과 燃料棒의 모델을 作成하였고, 이들 모델을 實驗을 通해 立證하였다. 有限要素모델과 SAPV電子計算 푸로그램을 使用하여 自然振動數와 모드를 求하였다. 核燃料棒의 $n=1$모드動特性을 쉽게 計算할 수 있는 간단한 보모델을 提示하였다. 보모델의 結果는 有限要素法에 依한것과 거의 비슷함을 보였다.

1. Introduction

Fuel rod failure due to vibration is a continuing concern for the design of liquid-cooled reactors. Mechanical wear at the contact regions between the fuel rod, grid dimples, and grid springs has been observed. Severe damages of fuel assemblies are reported due to impinging jet from baffle gap. Proven design methods for predicting fuel rod failure have not yet been developed because of the following reasons; 1) the dynamic characteristics of the fuel rod assembly are not adequately known, 2) the proper criteria for predicting the amount of wear have not been established and accurate values for wear coefficients and friction coefficients are not now available, 3) the basic excitation mechanisms causing fuel rod vibration have not yet been completely characterized.

A fuel assembly can vibrate in two main ways.[1] One is low frequency vibration of the fuel assembly as a beam on end supports, and the other is high-frequency vibration of each individual fuel rod as a beam on multiple grid supports. The former type of vibration will mainly occur during seismic or blow-down excitation and will not be discussed in this paper. The latter type of vibration is considered to be the main cause of fuel rod failure and wear occurring at the rod-grid contact regions.

Two types of mathematical models are presented. One is a single-span beam model in which a fuel rod is represented by a simply-supported single-span Bernoulli-Euler beam with a rotational spring at each end. A closed-form solution is given for the normal mode of this model, and the advantages and disadvantages of this model are discussed. The other model is a finite element model of prototype fuel rods that we use in SAP V[2] computer analyses of fuel rod dynamics. In this model, a fuel rod is represented by a set of finite elements consisting of a massless elastic beam of element-length with one-half of the element-mass concentrated at each end, and each grid is represented by a set of three springs representing the stiffnesses of the grid at the rod-grid contact regions. It is proved experimentally that the three-spring representation of a grid is a valid grid model for normal-mode analysis of prototype fuel rods.

2. Mechanical Characteristics of Grid Supports

2.1 Grid Supports

Prototype fuel rods are supported along their length by seven grid assemblies. Each grid assembly consists of a 17×17 array of grid cells.[3] Each cell has two springs and four dimples which are formed on the sides of the cell by a punching operation. A typical cell is shown in Fig. 1. The fuel rod is constrained axially only by the friction force in order to allow for thermal expansion and irradiation growth of the rod. The grid spring and dimples in the plane of vibration will be called in-plane (section AA of Fig. 1) spring and dimples, and the other set of grid spring and dimples will be called the side spring and dimples.

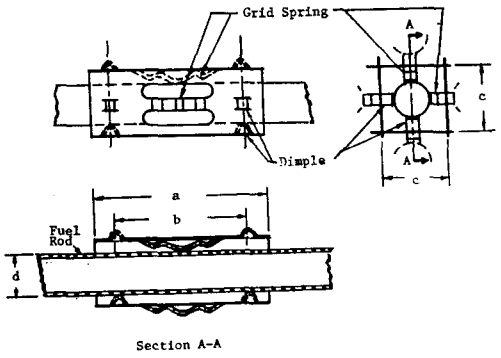

Fig. 1. Grid Cell

Since the mass of the spring and dimples is small compared with the modal mass of the fuel rod, we can represent each spring or dimple by a set of three weightless springs oriented perpendicularly to each other and corresponding to the stiffnesses in the radial, tangential, and axial directions with respect to the fuel rod. Hence, 18 springs are needed for a complete representation of one grid.

To simplify the problem, we will make the following assumptions; 1) the fuel rod always vibrates in a plane perpendicular to one of the walls in which the dimples are located, 2) the grids springs and dimples remain in contact with the fuel rod during the vibration, 3) the axial stiffnesses of the grid spring and dimples will have negligible effect on the vibration characteristics of a fuel rod. Then, the equivalent stiffnesses of the springs and dimples are

$$K_D = K_{dr} + K_{dt} \qquad (1)$$
$$K_S = K_{sr} + K_{st}$$

where K_D is the equivalent dimple stiffness, K_S is the equivalent spring stiffness, and K_{dr}, K_{dt}, K_{sr}, and K_{st} are the radial dimple, tangential dimple, radial spring, and tangential spring stiffnesses, respectively. The location and stiffness of each of these

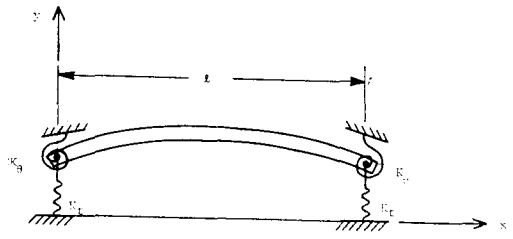

(b) **Single-Span Beam Model**

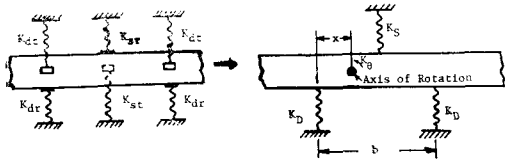

(a) **Mathematical Model of Grid Cell**

Fig. 2. Mathematical Model of Grid Cell and Single Span Beam Model

idealized springs correspond to those of the actual grid springs and dimples, as shown in Fig. 2a. Thus, each grid is represented by three springs, two K_D springs spaced apart a distance b and a K_S spring located midway between them.

Measurement of the static tangential stiffnesses is almost impossible because of its geometry and size. Therefore semi-emperical methods were used. The following models were used for the purpose.

1. Model 3—19=Three-span test model, span length= .483m
2. Model 1—25=Single-span test model, span length= .635m
3. Model 1—25SDR=Modle 1—25 with side spring and dimple removed.

The average spacing between each grid spring and corresponding dimples was adjusted to ensure the spring preload is approximately equal to 27N. The bending rigidities EI of the test tubes were determined from natural frequency tests. A clamped-free boundary condition was used for its simplicity. For a clamped-free beam $(\beta_1 l)^2$ in Eq. 16 is 3.5160.[4] Hence $EI=0.507\mu l^4$ where μ is the mass per unit length and l is the length of the cantilever. To improve accuracy, several different lengths were adopted for the test. The values were found to be; $EI=22.4\text{N.m}^2$, $\mu=0.127\text{kg/m}$ for an empty Zircaloy tube, and $EI=26.7\text{N.m}^2$, $\mu=0.870\text{kg/m}$ for a depleted fuel rod with 130N axial load and 1.73MPa at room temperature.

2.2 Stiffnesses of Grid Supports

The static radial stiffnesses of the grid spring and dimples of a prototype grid were measured using an Instron Uuiversal Testing Machine. The edges of the spring and dimple base plates were welded to a recessed steel block. The radial dimple stiffness K_{dr} is linear in the displacement range of interest and has the value

$$K_{dr}=5.46\times10^5\text{N/m} \qquad (2)$$

The radial stiffness K_{sr} of the grid spring is linear for small displacement and becomes non-linear for large displacement.

$$K_{sr}=8.9\times10^4\text{N/m for } y<.3\text{mm} \qquad (3)$$
$$=3.5\times10^4\text{N/m for } y>.5\text{mm}$$

These results indicate that the spring stiffness will change as the spring preload changes. However, this is of minor importance since K_{sr} is much smaller than K_{st}.

A SAP V analysis was made on model 1—25 SDR using the statically determined radial stiffness values given in Eqs. 2 and 3. The calculated natural frequency of 83.9 Hz agrees very well with the measured value of 84Hz as is seen in Table 1. Therefore, it was concluded that the statically measured radial stiffness values and three spring representation of a grid are valid for dynamic analyses of fuel rods.

The measured natural frequencies of the test models are compared with SAP V

Table 1. Comparison of Test and SAP V Analysis

Model No.	Mode	Frequencies, Hz		Rotational Stiffness K_θ N.m/rad	
	n	Measured	SAP V	Nominal	Equivalent
1-25SDR	1	84.0	83.9	$\frac{K_D b^2}{2}=220$	240
	2	—	248.3		
1-25	1	99.8	100.6	$\frac{K_D b^2}{2}=630$	700
	2	—	281.6		
	3	—	557.9		
3-19	1	153.4	155.1	$\frac{K_D b^2}{2}=310$	400
	2	175.3	171.2		
	3	199.7	192.7		

results in Table 1. Model 1—25 has 19% higher fundamental natural frequency than does model 1—25SDR because of the tangential stiffnesses of the side grid dimples and spring. The equivalent translational dimple stiffness used in SAP V analysis was deduced by the semi-emperical method described in the Appendix. They are

$$K_D=K_{dt}+K_{dr}=1.55\times10^6 \text{ N/m} \quad (4)$$
$$K_S=K_{st}+K_{sr}=1.00\times10^5 \text{ N/m}$$

The stiffnesses of a structure are temperature-dependent due to the temperature-dependence of Young's modulus E. Young's modulus of Inconel 718 is reduced by 5% at the operating temperature 316°C. Therefore, the stiffness values to be used for dynamic analyses of prototype fuel rods at normal operating temperatures are

$$K_D=1.458\times10^6\text{N/m}$$
$$K_S=9.30\times10^4\text{N/m}$$
$$K_{dt}=9.33\times10^5\text{N/m} \quad (5)$$
$$K_{dr}=5.25\times10^5\text{N/m}$$
$$K_{st}=6.00\times10^4\text{N/m}$$
$$K_{st}=3.30\times10^4\text{N/m}$$

3. Multi-Span Fuel Rods

Tables for calculating the natural frequencies of a continuous beam on equally spaced simple supports are available.[5,6] However, the natural frequencies and mode shapes of a beam on multiple unequally spaced supports or on equally spaced but more complicated supports (spring constraints) have to be calculated case by case.

3.1 Finite-Element Fuel Rod Models

The fuel rod, which has distributed mass and elasticity, can be modeled by finite elements. A portion of the fuel rod of length Δl is represented by a weightless rod of the same geometry and elasticity as the fuel rod with one-half of the mass of each section lumped at each end of the section as shown in Figs. 3a and 3b. For a typical prototype fuel rod span shown in Fig. 3c.

$$\mu_1=(l-0.0286)\mu/8$$
$$\mu_2=(l-0.0286)\mu+0.0143\mu/2$$
$$\mu_3=0.0143\mu$$
$$\mu_4=l_e\mu/2$$
$$\mu_5=(l_e-0.0143)\mu/2$$

The grid spring and dimples are modeled by three translational springs K_D, K_S, and K_D. The span between adjacent grids is represented by ten finite elements as shown in Fig. 3 and in Table 4, The fuel rod geometries considered are the prototype six span fuel rod, Model 6—26, in addition to models 3—19 and 1—25.

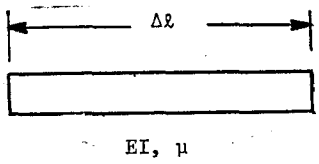

(a) Element of Rod with Distributed Mass

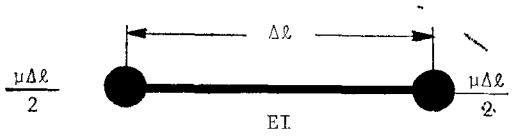

(b) Finite Element Model of (a)

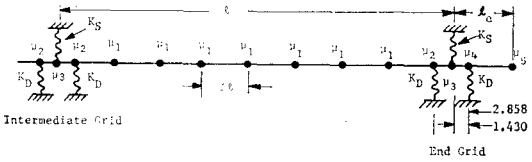

(c) Finite Element Model of a Typical Fuel Pod

Fig. 3. Finite Element Model of a Typical Fuel Rod Span

3.2 Natural Frequencies and Mode Shapes

The accuracy of the natural frequencies calculated using the finite element method depends on the finite element model adopted, the number of finite elements used, and the boundary conditions for the system to be analyed. In general, the accuracy improves as the number of finite elements increases. The results, however, should be checked either by experiment or by comparison with an exact solution if one is availabe. The accuracy depends on the number of finite element used and impedance matching for a shock response.[7,8] The rule of thumb for selecting the number of finite elements needed for good engineering accuracy (natural frequency accurate within 0.7%) of the natural frequencies of a singlespan beam is to take about 8n elements where n is the number of the highest mode of interest.

Each span of the multi-span fuel rod model takes on the fundamental mode shapes of a single-span beam having a variety of

Table 2. Mode Shapes of Test Model 1-25

Grid No.	Mass Points	Coordinates of Mass Points	Mode Shape	
			1	2
1	1	0.0	2.210965E-02	5.169385E-02
	2	1.429	−6.842096E-04	−9.207703E-03
	3	2.858	−2.789955E-02	−8.041608E-02
	4	8.922	−2.238563E-01	−5.311205E-01
	5	14.986	−4.913669E-01	−9.355967E-01
	6	21.050	−7.498465E-01	−1.000000E-01
	7	27.115	−9.337189E-01	−6.414098E-01
	8	33.179	−1.000000E-01	8.104025E-01
	9	39.243	−9.337189E-01	6.414098E-01
	10	45.307	−7.498465E-01	1.000000E-00
	11	51.371	−4.913669E-01	9.355967E-01
	12	57.436	−2.238563E-01	5.311205E-01
	13	63.500	−2.789955E-02	8.041608E-01
2	14	64.929	−6.842096E-04	9.207703E-03
	15	66.358	2.210965E-02	−5.169385E-02
Natural Frequency, Hz			100.6	821.6

Table 3. Mode Shapes of Test Model 3-19

Grid No.	Mass Points	Coordinates of Mass Points	Mode Shape		
			ϕ_1	ϕ_2	ϕ_3
1	1	0.0	2.449E-02	3.379E-02	2.418E-02
	2	1.429	−1.825E-03	−2.906E-03	2.465E-03
	3	2.858	−3.304E-02	−4.636E-02	−3.394E-02
	4	10.424	−3.146E-01	−4.330E-01	−3.087E-01
	5	17.991	−6.252E-01	−8.396E-01	−5.781E-01
	6	25.558	−7.752E-01	−1.000E-01	−6.485E-01
	7	33.124	−9.802E-01	−8.199E-01	−4.748E-01
	8	40.693	−3.856E-01	−4.073E-01	−1.772E-01
	9	48.260	−5.095E-02	−3.862E-02	−1.406E-04
2	10	49.689	3.520E-04	−1.975E-03	−4.337E-03
	11	51.118	5.364E-02	2.529E-02	−2.546E-02
	12	58.648	4.514E-01	9.824E-02	−3.744E-01
	13	66.251	8.420E-01	7.644E-02	−8.117E-01
	14	73.818	1.000E-00	1.952E-05	−1.000E-00
	15	81.384	8.420E-01	−7.644E-02	−8.117E-01
	16	88.953	4.514E-01	−9.824E-02	−3.744E-01
	17	96.520	5.364E-02	−2.529E-02	−2.546E-02
3	18	97.949	3.519E-04	1.975E-03	−4.337E-03
	19	99.378	−5.095E-02	3.862E-02	−1.406E-04
	20	106.944	−3.856E-01	4.073E-01	−1.772E-01
	21	114.511	−6.801E-01	8.193E-01	−4.748E-01
	22	122.075	−7.752E-01	1.000E-00	−6.485E-01
	23	129.644	−6.253E-01	8.396E-01	−5.781E-01
	24	137.213	−3.146E-01	4.330E-01	−3.087E-01
	25	144.780	−3.304E-02	4.636E-02	−3.394E-02
	26	146.209	−1.825E-03	2.906E-03	−2.465E-03
	27	147.638	2.449E-02	−3.379E-02	2.418E-02
Natural Frequencies, Hz			155.1	171.2	192.7

different boundary conditions up to the n= N mode, where N is the number of spans. Therefore, by using eight finite elements for each span in our fuel rod models, the error in calculated natural frequency is less than 0.7% for the natural frequencies of the first N modes. Calculated natural frequencies for several fuel rod models are given in Tables 2, 3, and 4. The results show that the frequencies are very close to each other up to the Nth mode. This indicates that it is difficult to detune the rod if the excitation frequencies are in this range. The fundamental natural frequency of a fuel rod on many un-equally spaced supports is strongly influenced by the longest span, when the number of supports, total length, and the physical properties are the same. In particular, the fundamental natural frequency of a rod on equally spaced supports is higher than that of the same rod on unequally spaced supports.

For a finite element solution, the error in mode shape is greater than the error in natural frequency due to discontinuities in slope that occur at each connection point. An exact error criterion is not available. However, it is believed that the mode-shape

Table 4. Mode Shapes of Prototype Six-Span Fuel Rod

Grid No.	Mass Points	Normalized Coordinates	Mode Shape						
			ϕ_1	ϕ_2	ϕ_3	ϕ_4	ϕ_5	ϕ_6	ϕ_7
	1	0.0	5.713E-03	3.056E-02	4.089E-02	4.942E-02	1.249E-01	5.926E-05	1.727E-02
1	2	1.640	1.070E-03	5.697E-03	7.593E-03	9.124E-03	2.287E-02	1.012E-05	2.822E-03
	3	2.009	−4.277E-06	−4.536E-05	−8.657E-05	−1.492E-04	−5.396E-04	−7.671E-07	−2.790E-04
	4	2.081	−1.308E-03	−7.008E-03	−9.365E-03	−1.136E-02	−2.876E-02	−1.356E-05	−3.854E-03
	5	4.279	−1.397E-02	−7.419E-02	−9.865E-02	−1.181E-01	−2.944E-01	−1.231E-04	−3.278E-02
	6	6.178	−3.172E-02	−1.671E-01	−2.204E-01	−2.610E-01	−6.400E-01	−2.325E-04	−5.690E-02
	7	8.078	−4.797E-02	−2.497E-01	−3.261E-01	−3.801E-01	−9.100E-01	−2.633E-04	−5.478E-02
	8	9.978	−5.755E-02	−2.948E-01	−3.794E-01	−4.326E-01	−1.000E-00	−1.893E-04	−2.432E-02
	9	11.878	−5.739E-02	−2.875E-01	−3.625E-01	−4.004E-01	−8.773E-01	−4.381E-05	1.806E-02
	10	13.779	−4.691E-02	−2.230E-01	−2.790E-01	−2.934E-01	−5.879E-01	9.740E-05	4.775E-02
	11	15.679	−2.806E-02	−1.305E-01	−1.526E-01	−1.477E-01	−2.470E-01	1.479E-04	4.599E-02
	12	17.579	−4.826E-03	−2.090E-02	−2.256E-02	−1.842E-02	−1.703E-02	4.082E-05	9.713E-03
2	13	17.948	−6.156E-05	−1.710E-04	−1.036E-04	−1.083E-05	−8.393E-05	−3.205E-06	−8.235E-04
	14	18.317	5.699E-03	2.416E-02	2.528E-02	1.890E-02	8.138E-03	−6.384E-05	−1.426E-02
	15	20.331	6.754E-02	2.753E-01	2.743E-01	1.793E-01	−4.775E-02	−7.287E-04	−1.460E-01
	16	22.445	1.529E-01	6.109E-01	5.949E-01	3.661E-01	−1.993E-01	−1.391E-03	−2.499E-01
	17	24.509	2.265E-01	8.864E-01	8.447E-01	4.949E-01	−3.512E-01	−1.480E-03	−2.153E-01
	18	26.572	2.622E-01	1.000E-00	9.282E-01	5.144E-01	−4.305E-01	−8.570E-04	−4.760E-02
	19	28.636	2.480E-01	9.121E-01	8.155E-01	4.176E-01	−4.029E-01	1.606E-04	1.486E-01
	20	30.700	1.874E-01	6.521E-01	5.485E-01	2.437E-01	2.806E-01	9.933E-04	2.470E-01
	21	32.764	9.909E-02	3.127E-01	2.324E-01	6.949E-02	−1.198E-01	1.104E-03	1.889E-01
	22	34.828	1.298E-02	3.271E-02	1.581E-02	−5.571E-03	−7.547E-03	2.458E-04	2.892E-02
3	23	35.197	8.773E-05	−3.663E-05	−2.083E-04	−1.404E-04	−3.407E-05	−1.596E-05	−1.202E-03
	24	35.566	−1.424E-02	−3.200E-02	−1.018E-02	1.374E-02	3.757E-03	−3.602E-04	−3.554E-02
	25	37.630	−1.530E-01	−2.834E-01	−5.846E-03	2.453E-01	−1.782E-02	−3.980E-03	−3.318E-01
	26	39.694	−3.359E-01	−5.721E-01	6.376E-02	5.967E-01	−8.002E-02	−7.511E-03	−5.450E-01
	27	41.759	−4.890E-01	−7.840E-01	1.535E-01	8.895E-01	−1.433E-01	−7.921E-03	−4.503E-01
	28	43.822	−5.590E-01	−8.451E-01	2.236E-01	1.000E-00	−1.773E-01	−4.516E-03	−7.557E-02
	29	45.886	−5.225E-01	−7.359E-01	2.465E-01	8.846E-01	−1.673E-01	9.709E-04	3.444E-01
	30	47.950	−3.897E-01	−4.953E-01	2.117E-01	5.889E-01	−1.177E-01	5.414E-03	5.403E-01
	31	50.014	−2.022E-01	−2.136E-01	1.279E-01	2.384E-01	−5.119E-02	5.950E-03	3.997E-01
	32	52.078	−2.552E-02	−1.606E-02	2.000E-02	1.222E-02	−3.516E-03	1.308E-03	5.844E-02
4	33	52.447	−7.152E-05	2.138E-04	5.097E-05	−1.018E-04	−1.623E-05	−9.697E-05	−2.415E-03
	34	52.816	2.771E-02	1.200E-02	−2.377E-02	−3.482E-03	2.079E-03	−1.939E-03	−7.028E-02
	35	54.879	2.895E-01	4.484E-02	−2.718E-02	9.445E-02	−6.682E-04	−2.106E-02	−6.326E-01
	36	56.944	6.252E-01	3.521E-02	−5.950E-01	2.962E-01	−1.799E-02	−3.883E-02	−9.992E-01
	37	59.008	8.944E-01	−1.091E-03	−8.410E-01	4.846E-01	−3.758E-02	−3.905E-02	−7.574E-01
	38	61.072	1.000E-00	−4.575E-02	−9.104E-01	5.732E-01	−4.945E-02	−1.907E-02	−1.312E-02
	39	63.135	9.058E-01	−8.072E-02	−7.768E-01	5.247E-01	−4.827E-02	1.036E-02	7.396E-01
	40	65.199	6.434E-01	−9.146E-02	−4.932E-01	3.595E-01	−3.471E-02	3.195E-02	1.000E-00
	41	67.263	3.060E-01	−6.966E-02	−1.803E-01	1.509E-01	−1.536E-02	3.176E-02	6.461E-01
	42	69.328	3.145E-02	−1.393E-02	−3.294E-03	8.999E-03	−1.087E-03	6.507E-03	7.444E-02
5	43	69.696	−5.380E-05	−1.351E-04	2.139E-04	−6.733E-06	−1.064E-05	−4.272E-04	1.558E-03
	44	70.065	−3.047E-02	1.767E-02	−6.803E-03	−4.067E-03	6.546E-04	−9.326E-03	−6.632E-02
	45	72.129	−2.649E-01	2.200E-01	−2.123E-01	3.256E-02	2.453E-04	−9.978E-02	−4.782E-01
	46	74.194	−5.311E-01	4.975E-01	−5.576E-01	1.248E-01	−4.421E-03	−8.828E-01	−6.588E-01
	47	76.258	−7.256E-01	7.228E-01	−8.633E-01	2.170E-01	−9.941E-03	−1.830E-01	−4.131E-01
	48	78.321	−7.816E-01	8.081E-01	−1.000E-00	2.670E-01	−1.349E-02	−8.837E-02	1.143E-01
	49	80.385	−6.813E-01	7.220E-01	−9.138E-01	2.517E-01	−1.348E-02	5.010E-02	5.680E-01
	50	82.449	−4.603E-01	4.963E-01	−6.377E-01	1.797E-01	−9.961E-03	1.511E-01	6.514E-01
	51	84.513	−2.005E-01	2.189E-01	−2.843E-01	8.138E-02	−4.621E-03	1.495E-01	3.597E-01
	52	86.577	−1.576E-02	1.743E-02	−2.292E-02	6.675E-03	−3.893E-04	3.084E-02	2.827E-02
6	53	86.946	1.698E-04	−1.189E-04	8.091E-05	6.375E-06	−2.711E-06	−1.610E-03	3.879E-03
	54	87.315	1.232E-02	−1.358E-02	1.780E-02	−5.168E-03	3.009E-04	−4.330E-02	−7.595E-03
	55	88.546	4.382E-02	−4.836E-02	6.472E-02	−1.910E-02	1.141E-03	−2.743E-01	1.960E-02
	56	89.778	6.395E-02	−7.184E-02	9.584E-02	−2.860E-02	1.739E-03	−5.708E-01	1.088E-01
	57	91.010	7.335E-02	−8.293E-02	1.113E-01	−3.351E-02	2.068E-03	−8.344E-01	2.130E-01
	58	92.241	7.314E-02	−8.314E-02	1.121E-01	−3.401E-02	2.124E-03	−9.906E-01	2.928E-01
	59	93.473	6.505E-02	−7.426E-02	1.005E-01	−3.068E-02	1.934E-03	−1.000E-00	3.221E-01
	60	34.705	5.134E-02	−5.881E-02	7.987E-02	−2.448E-02	1.554E-03	−8.641E-01	2.937E-01
	61	96.792	2.322E-02	−2.670E-02	3.639E-02	−1.121E-02	7.177E-04	−4.313E-01	1.545E-01
	62	98.880	1.967E-03	−2.269E-03	3.102E-03	−9.600E-04	6.186E-05	−3.945E-02	1.465E-02
7	63	99.249	1.895E-05	−2.470E-05	3.720E-05	−1.308E-05	9.960E-07	−1.485E-03	7.348E-04
	64	99.617	−1.581E-03	1.819E-03	−2.481E-03	7.652E-04	−4.906E-05	2.992E-05	−1.082E-02
	65	100.0	−3.177E-03	3.660E-03	−4.995E-03	1.542E-03	−9.904E-05	6.131E-02	−2.238E-02
Normalized Natural Frequency			1.00	1.05	1.14	1.22	1.35	2.31	2.87

error is less than 10% for the finite element model used. The normalized mode shapes for fuel rod models 1-25, 3-19, and 6-25 are given in Tables 2, 3 and 4, respectively.

4. Single-Span Fuel Rod Model

4.1 Spring Stiffness

An approximate model for an intermediate span of a multi-span fuel rod is shown in Fig. 2b. In this model, the three grid springs are replaced by two equivalent springs, one translational and the other rotational. The total equivalent translational spring stiffness of a grid is

$$K_t=2K_D+K_S \tag{6}$$

where K_D and K_S are given by Eq. 1. The equivalent rotational stiffness of the grid is a function of the location of the axis of rotation. If the axis of rotation is at distance x from one of the dimples, then the rotational stiffness of the grid is

$$k_\theta=\frac{F_\theta}{\theta}=K_D(b^2-2bx+2x^2)+K_S\left(\frac{b}{2}-x\right)^2 \tag{7}$$

where F_θ is the applied moment, θ is the resulting angle of rotation, and b is the distance between dimples. During vibration of a multi-span fuel rod in any particular mode, the deflected shapes of the various adjacent spans are often considerably different (see Fig. 5, for example) so that the inertia forces acting on the rod on each side of a grid are different and the axis of the rotation is not located at $x=b/2$. The location of the axis of rotation relative to the grid midpoint is different for different grids and different modes. However, for simplicity we will assume that $x=b/2$ when calculating the rotational stiffness. Substituting $x=b/2$ into Eq. 7 we find the approximate total rotational stiffness of a grid to be

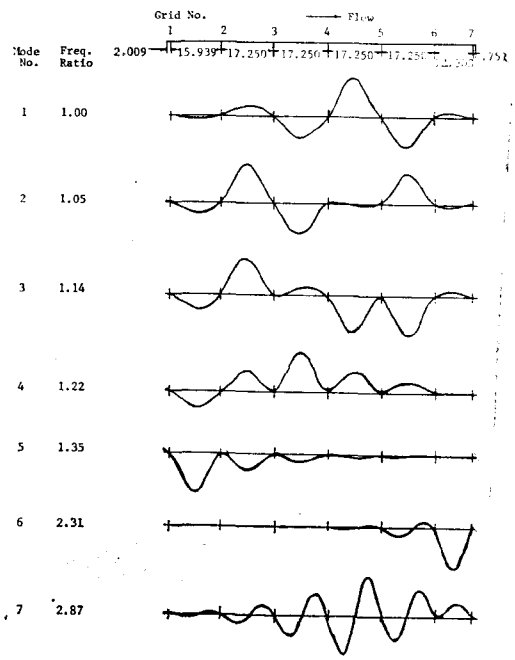

Fig. 5. Natural Frequencies and Mode Shapes of the Prototype Six-Span

$$k_\theta=\frac{K_Db^2}{2} \tag{8}$$

Since half of the translational and rotational stiffnesses of a grid act on each adjacent span of a multispan fuel rod that is vibrating symmetrically, only half of the total stiffnesses of a grid are used for the single-span models. That is

$$K_\theta=\frac{k_\theta}{2},\quad K_t=\frac{k_t}{2} \tag{9}$$

where K_θ and K_t are the equivalent rotational and translational stiffnesses, respectively. The model shown in Fig. 2 accurately represents a multi-span fuel rod for which the stiffnesses of the grids at each end are one-half as stiff as the intermediate grids, and for which the span lengths are equal and the rod is vibrating in its fundamental mode. This model only approximately represents a multi-span fuel rod for which the

end grids have the same stiffnesses as the intermediate grids.

4.2 Natural Frequencies and Mode Shapes

Equation of motion for the Bernoulli-Euler[10] beam shown in Fig. 2b is given by

$$\frac{\partial^2}{\partial x^2}\left(EI\frac{\partial^2 y}{\partial x^2}\right)+\mu\frac{\partial^2 y}{\partial t^2}=0 \qquad (10)$$

where EI and μ are the bending rigidity and mass per unit length of the beam, respectively. For a constant EI and an undamped free vibration, we substitute $y(x,t)=Y(x)\cdot e^{i\omega t}$ into Eq. 10 and find

$$\frac{d^4Y}{dx^4}-\beta^4 Y=0,\quad \beta^4=\mu\omega^2/EI \qquad (11)$$

A general solutions of Eq. 11 is well known

$$Y(x)=A_1C_1+A_2S_1+A_3C_2+A_4S_2 \qquad (12)$$

where $C_1=\mathrm{Cosh}(\beta x)+\mathrm{Cos}(\beta x)$,

$C_2=\mathrm{Cosh}(\beta x)-\mathrm{Cos}(\beta x)$

$S_1=\mathrm{Sinh}(\beta x)+\mathrm{Sin}(\beta x)$,

$S_2=\mathrm{Sinh}(\beta x)-\mathrm{Sin}(\beta x)$

and Ai are the integration constants to be determined from boundary conditions. The boundary conditions for the single-span model are;

$$\text{at}\quad x=0\quad EI\frac{d^2Y}{dx^2}=K_\theta\frac{dY}{dx},\quad EI\frac{d^3Y}{dx^3}=-K_tY \qquad (13)$$

$$\text{at}\quad x=l\quad EI\frac{d^2Y}{dx^2}=-K_\theta\frac{d^2Y}{dx^2},\quad EI\frac{d^3Y}{dx^3}=K_tY$$

From Eqs. 12 and 13, we obtain four homogeneous equations for four unknowns Ai. For non-trivial solution, the determinant of coefficients of Ai must vanish, from which we obtain the frequency equation of the model. The equation is

$$\left[1+\left(\frac{K_\theta l}{EI}\right)\left(\frac{K_t l^3}{EI}\right)\frac{1}{(\beta l)^4}\right]^2\times [1-\mathrm{Cosh}(\beta l)\ \mathrm{Cos}(\beta l)]$$
$$-2\left(\frac{K_\theta l}{EI}\right)\frac{1}{(\beta l)}\left[1-\left(\frac{K_\theta l}{EI}\right)\left(\frac{K_t l^3}{EI}\right)\frac{1}{(\beta l)^4}\right]\times [\mathrm{Cosh}(\beta l)\mathrm{Sin}(\beta l)+\mathrm{Sinh}(\beta l)\mathrm{Cos}(\beta l)]$$
$$-2\left(\frac{K_t l^3}{EI}\right)\frac{1}{(\beta l)^3}\left[1-\left(\frac{K_\theta l}{EI}\right)\left(\frac{K_t l^3}{EI}\right)\frac{1}{(\beta l)^4}\right]\times [\mathrm{Cosh}(\beta l)\mathrm{Sin}(\beta l)-\mathrm{Sinh}(\beta l)\mathrm{Cos}(\beta l)]$$
$$+4\left(\frac{K_\theta l}{EI}\right)\left(\frac{K_t l^3}{EI}\right)\frac{1}{(\beta l)^4}\cdot\mathrm{Cosh}(\beta l)\mathrm{Cos}(\beta l)$$
$$-2\frac{1}{(\beta l)^2}\left[\left(\frac{K_\theta l}{EI}\right)^2-\left(\frac{K_t l^3}{EI}\right)^2\frac{1}{(\beta l)^4}\times \mathrm{Sinh}(\beta l)\ \sin(\beta l)=0\right. \qquad (14)$$

It can be noted the frequency equation is essentially a weighted sum of a number of frequency equations for beams with more elementary boundary conditions. When the numerical values appropriate for the fuel rod are used, it can be shown that the analysis can be simplified without significant error by setting K_t equal to infinity for the present fuel rod assemblies. Then Eq. 14 reduces to

$$2\left(\frac{EI}{K_\theta l}\right)^2(\beta l)^2\mathrm{Sinh}(\beta l)\mathrm{Sin}(\beta l)+2\left(\frac{EI}{K_\theta l}\right)(\beta l)\ [\mathrm{Cosh}(\beta l)\mathrm{Sin}(\beta l)-\mathrm{Sinh}(\beta l)\mathrm{Cos}(\beta l)]+[1-\mathrm{Cosh}(\beta l)\mathrm{Cos}(\beta l)]=0 \qquad (15)$$

the frequency of the nth mode is

$$f_n=\frac{(\beta_n l)^2}{2}\sqrt{\frac{EI}{\mu l^4}} \qquad (16)$$

where $\beta_n l$ is the nth root of Eq. 15. The eigen value is plotted for $n=1$ and 2 in Fig.4 as a function of the stiffness parameter λ

$$\lambda=\left[1+\frac{EI}{K_\theta l}\right]^{-1} \qquad (17)$$

The normalized mode shapes $\phi_n(\beta_n x)$ of a single-span beam having a rotational spring at each end ($K_t=\infty$) are

$$\phi_n(\beta_n x)=\frac{1}{\phi^*}\{-\mathrm{Sinh}(\beta_n x)+\mathrm{Sin}(\beta_n x)+\zeta_n(\mathrm{Sinh}(\beta_n x)+\mathrm{Sin}(\beta_n x)+\frac{K_\theta l}{EI}\frac{1}{(\beta l)}[\mathrm{Cosh}(\beta_n x)-\mathrm{Cos}(\beta_n x)])\} \qquad (18)$$

and

$$\zeta_n=\{\mathrm{Sinh}(\beta_n l)-\mathrm{Sin}(\beta_n l)\}/\{\mathrm{Sinhn}(\beta_n l)$$

$$+\mathrm{Sin}(\beta_n l)$$
$$+\frac{K_\theta l}{EI}\frac{1}{(\beta_n l)}[\mathrm{Cosh}(\beta_n l)-\mathrm{Cos}(\beta_n l)]\}$$

where the normalization factor ϕ^* is equal to the maximum value of the expression in the brackets in Eq. 18. It decreases monotonically from 2 to 1.616 as λ increases from 0 to 1. Angle of rotation at the grids are of great importance in calculating forces acting on the dimples. Derivetives of Eq. 18 at $x=0$ or l render

$$\frac{\theta_1 l}{y_1}=-(\beta_1 l)^2\left[\mathrm{Cosh}\left(\frac{\beta_1 l}{2}\right)-\mathrm{Cos}\left(\frac{\beta_1 l}{2}\right)\right]$$
$$\div\left\{\beta_1 l\left[\mathrm{Cosh}\left(\frac{\beta_1 l}{2}\right)\mathrm{Sin}\left(\frac{\beta_1 l}{2}\right)\right.\right.$$
$$\left.-\mathrm{Sinh}\left(\frac{\beta_1 l}{2}\right)\mathrm{Cos}\left(\frac{\beta_1 l}{2}\right)\right] \qquad (19)$$
$$\left.+\frac{K_\theta l}{EI}\left[1-\mathrm{Cosh}\left(\frac{\beta_1 l}{2}\right)\mathrm{Cos}\left(\frac{\beta_1 l}{2}\right)\right]\right\}$$

where θ_1 is the angle of rotation at $x=l$ for $n=1$ mode, y_1 is the maximum vibration amplitude, and l is the span length. Eq. 19 is plotted in Fig. 4 as a function the stiffness parameter λ. Let us calculate the fundamental natural frequency and dimple motion for model 1-25. The numerical values used for SAP V analysis are: $EI=22.4\mathrm{N.m^2}$, $l=0.635\mathrm{m}$, $\mu=0.127\mathrm{kg/m}$ and $K_D=1.55\times10^6$ N/m. Substituting into Eqs. 9 and 17, we find $K_\theta=630\mathrm{N.m/rad}$, and $\lambda=[1+EI/K_\theta l]^{-1}=0.947$. From Fig 4, we obtain $\beta_1 l=4.34$, and $\theta_1 l/y_1=1.05$. Then the natural frequency f_1 is

$$f_1=\frac{\beta_1 l^2}{2\pi}\sqrt{\frac{EI}{\mu l^4}}=98.8\mathrm{Hz}$$

Dimple displacement d_1 for $y_1=1$ can be obtained as follows

$$d_1=\left(\frac{\theta_1 l}{y_1}\right)\left(\frac{y_1}{l}\right)\left(\frac{b}{2}\right)$$
$$=1.05\times\frac{1}{0.635}\times0.01429=0.024$$

Note that $b/2$=coordinate of mass point 2 in Table 2. SAP V analysis show $f_1=100.6$ Hz and $d_1=0.027$ as in Table 2. There are only 2% difference in natural frequency and 13% defference in dimple displacement.

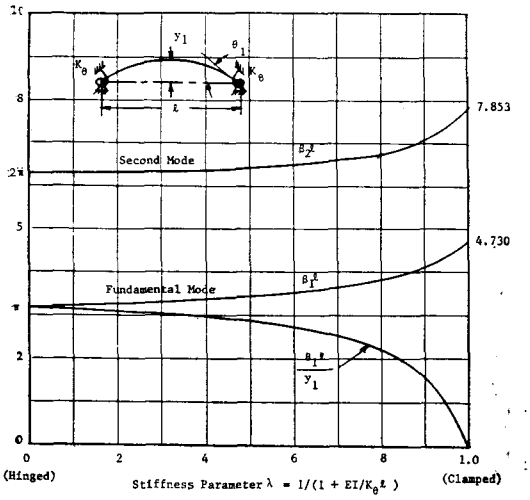

Fig. 4. Natural Frequencies and Angle of Rotation

5. Conclusions

1. There are 6 "fundamental" modes for the 6-span fuel rod. When a mode shape has a single loop per span, it is called a fundamental mode. The ranges of the normalized fundamental natural frequencies are 1-2.87. In particular the first 3 fundamental frequencies are 1, 1.05 and 1.14 respectively. Greater difficulties are anticipated for detuning if the rods are excited in this range.

2. The static stiffnesses of the grid spring and dimples can be used in computer analysis of prototype fuel rods on multiple grid supports. The measured and deduced values are

Radial Stiffness of Dimple$=K_d$,
$=5.25\times10^5\mathrm{N/m}$
Tangential Stiffness of Dimple
$=K_{dt}=9.33\times10^5\mathrm{N/m}$
Radial Stiffness of Spring$=K_{sr}$
$=3.3\times10^4\mathrm{N/m}$
Tangential Stiffness of Spring$=K_{st}$

$=6.0\times10^4$N/m

3. The single-span beam model can be used for calculating the lowest natural frequency and corresponding mode shape of prototype fuel rods. It is not accurate, however, for analyses of the higher modes.

Appendix: Deduction of Tangential Stiffnesses

The equivalent rotational stiffness K_θ in Fig. 2b. at the grids of model 1-25SDR can be calculated from the measured fundamental natural frequency as follows.

1. Calculate the fundamental natural frequency of a simply-supported Zircaloy tube that is 0.635m long.

$$f_1=\frac{\pi^2}{2\pi}\sqrt{\frac{EI}{\mu l^4}}=51.7\ \text{Hz} \qquad (A.1)$$

2. Calculate the frequency parameter $\beta_1 l$ corresponding to the fundamental natural frequency of 84.0Hz. From Eqs. Al and 16 we find that

$$\beta_1 l=\pi\sqrt{\frac{84.0}{51.7}}=4.00 \qquad (A.2)$$

3. Find the corresponding stiffness parameter from Fig.4.

$$\left(1+\frac{EI}{K_\theta l}\right)^{-1}=.87 \qquad (A.3)$$

4. Solving Eq. A3 for K_θ, we obtain

$$K_\theta\simeq240\text{N.m/rad} \qquad (A.4)$$

In a similar manner we will now calculate the equivalent rotational stiffness at the grids of model 1-25. Thus, $\beta_1 l=\pi\sqrt{99.8/51.8}=4.36$; from **Fig.4** we obtain $\lambda=.95$, so that

$$K_\theta=670\text{N.m/rad} \qquad (A.5)$$

The equivalent rotational stiffness K_θ is given by Eq. 7; that is

$$\begin{aligned}K_\theta&=(K_{dr}+K_{dt})(b^2-2bx+2x^2) \qquad (A.6)\\&\quad+(K_{sr}+K_{st})(b/2-x)^2\\&\simeq(K_{dr}+K_{dt})(b^2-2bx+2x^2)\end{aligned}$$

where x is the distance of the axis of rotation measured from the left-hand side dimple, and b is the distance between dimples. If we assume that the axis of rotation of both models is at the same location, then

$$\frac{(K_\theta)1-25}{(K_\theta)1-25\text{SDR}}\simeq\frac{670}{240}=\frac{K_{dt}+K_{dr}}{0+K_{dr}}$$

or

$$K_{dt}=K_{dr}\left(\frac{670-240}{240}\right)=1.0\text{MN/m} \qquad (A.7)$$

For the tangential spring stiffness, we will take the same ratio (for present convenience and not on a logical basis). Thus,

$$K_{st}=K_{sr}\left(\frac{670-240}{240}\right)=6.3\times10^4\ \text{N/m} \qquad (A.8)$$

Therefore, the equivalent dimple and spring stiffnesses and K_D and K_S to be used for dynamic analyses of grids are

$$\begin{aligned}K_D&=K_{dt}+K_{dr}=1.5\times10^6\ \text{N/m} \qquad (A.9)\\K_S&=K_{st}+K_{sr}=1.0\times10^5\ \text{N/m}\end{aligned}$$

Acknowledgement:

The anthor wishes to thank Miss H.C Lee of Computer Center of KAERI for assiatance in formulating the program used for the analysis.

References

1. Y. Takada and T. Egusa, "Vibration of the Fuel Assembly of a Marine Reactor", *J. Nuclear Engineering & Design*, pp. 578-584, 1968.
2. SAP V, A Structural Analysis Program for Static and Dynamic Response of Linear Systems, Dept. of Civil Engg., University of Southern California, U.S.A.
3. Systems Manual, Pressurized Water Reactors, USNRC Inspection and Enforcement Training Center, 1978.
4. D. Young and R.P. Felgar Jr., "Tables of Characteristic Functions Representing Normal Modes of Vibration of a Beam", The University of Texas Publication No. 4913, July 1949.
5. R.S. Ayre and L.S. Jacobsen, "Natural Freq-

uencies of Continuous Beams of Uniform Span Length", *Trans. ASME*, **72**, pp.391-395, Dec. 1950.

6. J.N. Macduff and R.P. Felgar, "Vibration Design Charts", ASME Paper 56-A-75.
7. H. Lee, "Optimum Modelling of Strectures to Predict Dynamic Elastic Response", Ph. D. Dissertation, The Pennsylvania State University, pp. 19-20, 1966.
8. V.H. Neubert & H. Lee, "Finite Beam Elements for Dynamic Analysis", The Shock and Vibration Bulletin, Bulletin 41, pp. 51-60, 1970.
9. E.G. Passig, "End Slope and Fundamental Frequency of Vibrating Fuel Rods", *J. Nuclear Engineering & Design*, **14**, pp. 198-200, 1970.
10. W.T. Thomson, "Vibration Theory and Applications", Prentice-Hall, Inc., pp. 273, 1965.